Pitching airfoil subjected to high amplitude free stream oscillations

Christoph Strangfeld[1], Hanns F. Müller-Vahl[2], David Greenblatt[2],
Berend G. van der Wall[3], C. Navid Nayeri[1], C. Oliver Paschereit[1]

[1] Institute of Fluid Dynamics and Technical Acoustics, Technische Universität Berlin,
Müller-Breslau- Str. 8, 10623 Berlin, Germany

[2] Faculty of Mechanical Engineering, Technion - Israel Institute of Technology,
32000 Haifa, Israel

[3] Institute of Flight Systems, DLR Braunschweig,
Lilienthalplatz 7, 38108 Braunschweig, Germany

Abstract

An experimental investigation was carried out to quantify the aerodynamic lift acting on a NACA 0018 airfoil subjected to combined pitching and surging and to compare the results to established theories. A dedicated unsteady wind tunnel was employed that produces large surge amplitudes, and airfoil loads were estimated by means of unsteady surface mounted pressure measurements. In-phase and out-of-phase pre-stall pitching and surging cases were considered for different velocity amplitudes. When the flow was fully attached, satisfactory correspondence was observed between experiments and theory. However, differences were observed when trailing-edge separation was present; in particular the shedding of a trailing-edge vortex corresponded with discrepancies between the experiments and theory.

Nomenclature

α Angle of attack, deg
λ Wave length of the oscillating free stream, m
ρ Air density, kg/m^3
σ Amplitude of the oscillating free stream
τ Phase shift, deg
ϕ Phase angle, deg
ω Angular frequency of the free stream oscillation, 1/s
a Non-dimensional pitch axis relative to the mid chord
c Airfoil chord length, m
i Imaginary unit
k Reduced frequency
l Coefficients from Isaacs
m Wave number
u Free stream velocity, m/s
A Coefficient from van der Wall
C Non-dimensional coefficient
$C(k)$ Theodorsen function
$F(k)$ Real part of the Theodorsen function
$G(k)$ Imaginary part of the Theodorsen function
H Coefficient from van der Wall
J Bessel function of the first kind
L Lift per unit span, N
M Pitching moment per unit span, Nm
Re Reynolds-number

Subscript
l Lift
m Pitch moment
n Variable number
qs Quasi steady
s Steady

Operators
$\overline{()}$ Time averaged
$\Im$ Imaginary part
$\Re$ Real part

1 INTRODUCTION

During the first half of the 20th century, the study of unsteady aerodynamics was motivated by problems associated with wing flutter, the estimation of helicopter blade loads, and the effect of wind gusts on aeroplanes. These problems remain relevant today. Indeed, unsteady blade loads and blade vibrations are still important subjects of helicopter and wind turbine aerodynamics research [1]; and the blades of high speed modern helicopters can experience velocity amplitudes of more than 100% [2]. The interactions of the unsteady effects are not fully understood, hence a more precise predictions of the unsteady lift overshoot is required [3, 4]. Moreover, the recent and dramatic rise in wind energy demands robust design of wind turbines - whose blades are exposed to highly unsteady flows produced by, inter alia, yaw misalignments, atmospheric turbulence, and the earth boundary layer - for the prediction of maximum fatigue loads [5]. In addition, wind turbine noise is highly affected by unsteady aerodynamics and noise reduction is an important research field [1]. Even the less popular vertical axis wind turbine is fundamentally an unsteady machine. It is facing strong free stream and angle of attack variations. In the field of wind energy produc-

tion, designers of modern wind turbines try to avoid the occurrence of dynamic stall due to the strong fatigue loads. Nevertheless, also fully attached blades encountering free stream or angle of attack variations which generate remarkable unsteady extra lift. Hence, this unsteady extra lift has to taken into account for any reliable life time prediction of wind turbine blades.

The landmark NACA report by Theodorsen [6] provided a general analytical solution for airfoils encountering angle of attack oscillations and plunging motions. Assuming a potential flow in a steady stream, he calculated all velocity potentials and determined the unsteady circulation, where the wake vorticity is determined by the Kutta condition. He made use of the following simplifications: flat plate airfoil, two-dimensional incompressible potential flow without viscosity, a straight and flat non-deforming wake, small angle assumption, and fully attached flow.

The need for more accurate estimations of helicopter blade loads motivated Isaacs [7] to extend Theodorsen's work to include sinusoidal free stream oscillations. Based on Theodorsen's and Isaacs' approaches, Greenberg [8] developed a simplified solution for the dynamic lift of a flat plate in an oscillating free stream including an oscillating angle of attack and oscillating plunge motion. In 1991, van der Wall provided an extensive review of existing theoretical approaches and extended Isaacs' theory to harmonic plunge motion and unsteady angle of attack variations including arbitrary multiples of the free stream harmonic [9, 10]. He concluded that Isaacs' theory is the only "exact theory" without additional simplifications. Furthermore, he determined significant deviations between Greenberg's and Isaacs' theories for velocity oscillation amplitudes higher than 0.4. Recently, both approaches were experimentally validated for an unsteady free stream with a velocity oscillation amplitude of 50% [11].

In light of the advances described above, it is surprising that many of these theories have not been fully validated experimentally, especially for large free stream oscillation amplitudes [12]. Favier et al. [13] investigated a pitching airfoil in unsteady free stream. The wind tunnel generated high reduced frequencies and moderate velocity amplitudes. Although the airfoil lift with fully attached flow showed significant dynamic effects, a comparison to Isaacs' theory was not attempted. More recently, Granlund et al. [14] investigated a NACA 0009 experimentally over a broad range of reduced frequencies at relatively small velocity amplitudes of 0.1. It is not clear why this lack of validation exists, but it seems that the existing experimental facilities lack the large amplitude unsteady parameter range. Tunnels that produce an unsteady free stream are rare. The most common approach is to modify a standard steady wind tunnel to produce unsteady flows [15, 16, 17, 18, 19]. Some tunnels combine the independent capabilities of angle of attack and wind speed variation [20, 21, 22]. Recently, an unsteady wind tunnel was developed to produce large amplitude oscillations of the free stream and synchronised arbitrary angle of attack variations

[23]. Problems of fan stall, large inertial effects, and acoustic resonance were overcome during the initial design and testing phases. The tunnel proved to be ideally suited to validate large amplitude unsteady effects and, in particular, to assess the validity of theoretical approaches.

All unsteady experiments including the combined and sychronised generation of free stream and angle of attack oscillations are compared to the theories of Theodorsen, Isaacs and van der Wall.

2 THEORY

2.1 Unsteady lift overshoot in potential flow

Figure 1 depicts a schematic of the experimental setup. A symmetrical airfoil, a NACA 0018 (black line), is pitching periodically around the quarter chord position (green arrow). The airfoil is sinusoidally pitching to both positive and negative pre-stall angles of attack while the free stream is synchronously oscillating. The length of the blue arrows outlines the time varying velocity amplitude. The frequencies of these two oscillations are identical and any desired phase shift between the two can be obtained. Caused by these two unsteady effects (unsteady inflow, wing motion), the lift and the proportional circulation of the bound vortex sheet vary in time. According to Helmholtz' circulation theorem, the overall circulation in the global system has to remain constant. Thus, a circulation change of arbitrary strength at one time step requires the shedding of a vortex into the wake with opposite strength at this time step (red arrows in the wake). The shed wake vorticity induces normal velocities on the airfoil which are adapted by a further circulation change. Thus, the wake contributes to the lift generated. The higher the velocity amplitudes or the reduced frequencies, the larger the influence of the wake vorticity.

All further discussed unsteady lift theories to predict the lift of the airfoil in figure 1 are based on the same assumptions: The airfoil is modelled as a flat plate in an incompressible potential flow. Hence, no boundary layer, friction forces, diffusion or separation exist. The flow remains fully attached all the time. Furthermore, the airfoil is assumed to be two-dimensional to avoid any spanwise effects like tip vortices or curved wake forms. During the derivations of the closed form solution presented here, small disturbances are assumed. Thus, the airfoil is regarded to be thin and only small angles of attack are considered. In the case of an unsteady, sinusoidal free stream, the maximum amplitude of the velocity oscillation is limited to $\sigma \leq 1$ to prohibit back flow.

On the on hand, the theory of Theodorsen [6] is used to predict the unsteady lift and pitch moment due to various airfoil motions like pitching, vertical airfoil motion, or flap deflections at a constant free stream. In the following, only harmonic, sinusoidal pitch motions are considered. On the other hand, the theory of Isaacs [7] computes the unsteady lift and pitch moment of an airfoil at a constant angle of attack facing an unsteady free stream. The theory of Greenberg [8]

considers the same problem but due to the so-called high frequency assumption, this theory is limited to relatively small velocity ratios σ below 0.4 [10, 11]. However, Isaacs extended his theory to incorporate both degrees of freedom at the same time; an unsteady, sinusoidal free stream and pitching around midchord [24]. Based on this landmark report, van der Wall further extended the theory to include an arbitrary pitch axis, the integration of arbitrary harmonic pitch profiles, and arbitrary vertical airfoil motion [9]. This approach is the most general formulation and hence, it is discussed here in more detail. Equation 1 predicts the unsteady lift overshoot depending on the phase angle ϕ. The assumed free stream velocity profile is $u(\phi) = u_s(1 + \sigma \sin(\phi))$ whereas u_s describes the steady free stream velocity and σ the amplitude of the velocity oscillations. Besides σ, the reduced frequency $k = \frac{\omega c}{2 u_s}$ is the second govering input parameter in all above mentioned theories. It describes the ratio between the angular frequency ω, the airfoil chord c, and u_s and gives a measure of the degree of the unsteadiness of the system. In all further discussion, the frequency of the free stream oscillations and the pitch frequency is identical, hence only one global k is defined here. The angle of attack profile is determined via $\alpha(\phi) = \alpha_0[\bar{\alpha}_0 + \sum_{n=1}^{\infty}(\bar{\alpha}_{nS} \sin(n\phi) + \bar{\alpha}_{nC} \cos(n\phi))]$. The normalised distance of the pitch axis to midchord amounts to $a = -0.5$ for pitching around the quarter chord. The first square bracket in equation 1 expresses the non circulatory part of the unsteady lift overshoot. The circulatory part is outlined in the second square bracket of equation 1 and includes a summation from the first wave number $m = 1$ to infinity. It requires the real $\Re$ and imaginary part $\Im$ of l_m. The most general formulation of this coefficients is given by van der Wall [9]. It includes Bessel functions of the first kind J and the well known Theodorsen function $C(mk) = F(mk) + iG(mk)$ [6].

2.2 Theoretical approach of van der Wall, Isaacs, and Greenberg

$$
\begin{aligned}
\frac{C_l(\phi)}{C_{l,qs}(\phi)} =~ & \frac{1}{(1 + \sigma \sin(\phi))^2} 0.5k[(\sigma\bar{\alpha}_0 + \bar{\alpha}_{1S} + k(a\bar{\alpha}_{1C} \\
& - 0.5\sigma\bar{\alpha}_{2C})\cos(\phi) + (-\bar{\alpha}_{1C} + k(a\bar{\alpha}_{1S} \\
& - 0.5\sigma\bar{\alpha}_{2S})\sin(\phi) + \sum_{n=2}^{\infty} n(\bar{\alpha}_{nS} + nka\bar{\alpha}_{nC} \\
& + 0.5\sigma(\bar{\alpha}_{(n-1)C} - \bar{\alpha}_{(n+1)C}))\cos(n\phi) \\
& + \sum_{n=2}^{\infty} n(-\bar{\alpha}_{nC} + nka\bar{\alpha}_{nS} + 0.5\sigma(\bar{\alpha}_{(n-1)S} \\
& - \bar{\alpha}_{(n+1)S}))\sin(n\phi)] + \frac{1}{(1 + \sigma \sin(\phi))^2} \\
& [((1 + 0.5\sigma^2)\bar{\alpha}_0 + \sigma(\bar{\alpha}_{1S} - 0.5k((0.5 - a) \\
& \bar{\alpha}_{1C}) - 0.25\sigma\bar{\alpha}_{2C})) \cdot (1 + \sigma \sin(\phi)) \\
(1)\quad & + \sum_{m=1}^{\infty}(\Re(l_m)\cos(m\phi) + \Im(l_m)\sin(m\phi))]
\end{aligned}
$$

The most general formulation of the coefficients is given by van der Wall [9]. Equations 2 to 5 determine the desired parameters.

$$
\begin{aligned}
l_m =~ & -2m(i)^{-m} \sum_{n=1}^{\infty}[F_n(J_{n+m}(n\sigma) \\
& - J_{n-m}(n\sigma)) + iG_n(J_{n+m}(n\sigma) \\
(2)\quad & + J_{n-m}(n\sigma))]
\end{aligned}
$$

$$
(3)\quad F_n + iG_n = [C(nk)]n^{-2}(H_n + iH_n')
$$

The formulation of the coefficients H_n and H_n' in the equations 4 and 5 assumes implicitly an ordinary oscillating pitch motion of the kind $\alpha(\phi) = \alpha_0[\bar{\alpha}_0 + \bar{\alpha}_{1S} \sin(\phi) + \bar{\alpha}_{1C} \cos(\phi)]$. A more general formulation for arbitrary motions can be found in [9].

$$
\begin{aligned}
H_n =~ & \frac{J_{n+1} - J_{n-1}}{2}[\sigma\bar{\alpha}_0 - \bar{\alpha}_{1s} - k(0.5 - a)\bar{\alpha}_{1c}] \\
(4)\quad & - \frac{2J_n}{n\sigma}\bar{\alpha}_{1s}
\end{aligned}
$$

$$
\begin{aligned}
H_n' =~ & \frac{J_{n+1} - J_{n-1}}{n}\bar{\alpha}_{1c} \\
(5)\quad & + \frac{J_n}{\sigma}\left[\bar{\alpha}_{1c}(1 - \sigma^2) - k(0.5 - a)\bar{\alpha}_{1s}\right]
\end{aligned}
$$

If a constant angle of attack is assumed, equation 1 reduces to the formulation of Isaacs [7]. The quasi steady lift coefficient $C_{l,qs}$ does not change in time because the angle of attack is constant.

$$
\begin{aligned}
\frac{C_l(\phi)}{C_{l,qs}} =~ & \frac{1}{(1 + \sigma \sin(\phi))^2}[1 + 0.5\sigma^2 + \sigma(1 + \Im(l_1) \\
& + 0.5\sigma^2)\sin(\phi) + \sigma(\Re(l_1) + 0.5k)\cos(\phi) \\
(6)\quad & + \sigma \sum_{m=2}^{\infty}(\Re(l_m)\cos(m\phi) + \Im(l_m)\sin(m\phi))]
\end{aligned}
$$

The coefficients of the infinite sum reduce to the formulation of Isaacs as well [7].

$$
\begin{aligned}
l_m =~ & -m(-i)^m \sum_{n=1}^{\infty}[F_n(J_{n+m}(n\sigma) - J_{n-m}(n\sigma)) \\
(7)\quad & + iG_n(J_{n+m}(n\sigma) + J_{n-m}(n\sigma))]
\end{aligned}
$$

$$
(8)\quad \left.\begin{array}{c} F_n \\ G_n \end{array}\right\} = \frac{J_{n+1}(n\sigma) - J_{n-1}(n\sigma)}{n^2} \left\{\begin{array}{c} F(nk) \\ G(nk) \end{array}\right.
$$

In the contrary, if the amplitude of the free stream velocity oscillation is zero, equation 1 is equivalent to the formulation of Theodorsen [6]. The free stream velocity is constant in this case, therefore no multiples of the free stream oscillation amplitude has to be considered. Thus, the infinite sum reduces to one single term and only one Theodorsen function has to be evaluated

with $C(k) = F(k) + iG(k)$.

$$\frac{C_l(\phi)}{C_{l,qs}} = \alpha_0^{-1}[0.5k(\beta_0\cos(\phi) + ak\beta_0\sin(\phi))$$

$$+\alpha_0 + \beta_0\sin(\phi)F - k(0.5-a)\beta_0\sin(\phi)G$$

(9) $$+\beta_0\cos(\phi)G + k(0.5-a)\beta_0\cos(\phi)F]$$

Furthermore, equations 1, 6, and 9 depict the lift coefficient ratio as $\frac{C_l(\phi)}{C_{l,qs}(\phi)} = \frac{L(\phi)}{L_s(\phi)}(1 + \sigma\sin(\phi))^2$. This formulation is chosen here because it directly shows the net unsteady effects and eliminates the influences of quasi steady effects like free stream velocity variations. The steady lift $L_s = \pi\rho c u_s^2\alpha$ is determined by means of the well-known Kutta-Joukowski equation [25] where s is the airfoil span and rho is the air density. The span is s and the air density is ρ.

In all theories, the assumed unsteady free stream is sinusoidal. Consequently the angle of attack is phase shifted toward the free stream if the free stream oscillation and the pitch motion are out of phase (at an identical frequency). Hence, a second formulation of the angle of attack including explicitly the phase shift τ is used here $\alpha(\phi) = \alpha_s + \alpha_{amp}\sin(\phi + \tau) = \alpha_s + \alpha_{amp}(sin(\phi)cos(\tau) + \cos(\phi)sin(\tau))$. A comparison to the formulation of the coefficients of van der Wall yields the relationships $\alpha_0 = \alpha_s$, $\bar{\alpha}_0 = 1$, $\alpha_{1S} = \alpha_{amp}\cos(\tau)\alpha_s^{-1}$, and $\alpha_{1C} = \alpha_{amp}\sin(\tau)\alpha_s^{-1}$.

3 EXPERIMENTAL SETUP

Figure 2 depicts a sketch of the entire wind tunnel setup. The blow down wind tunnel possesses a cross-section of 0.61m by 1.004m and a 8:1 contraction ratio. The maximum free stream velocity is 55m/s with a turbulence level of less than 0.1%. The wind tunnel is powered by a revolutions per minute regulated 75kW radial blower. The blower is specifically designed to operate smoothly under stalled conditions, allowing for a dynamic variation of the wind tunnel speed by adjusting the cross-sectional area of the wind tunnel exit. The ceiling, floor, and side walls of the test section incorporating the airfoil are equipped with Plexiglas to ensure optimal optical access for PIV measurements. At the end of the 4.07m long test track louvers control the free stream velocity dynamically. The distance from the louvers to the trailing edge of the wing is 2.8m, which is sufficient to avoid a spatial inhomogenity of the flow field at the location of the airfoil model. The louver mechanism consists of 13 fully rotatable vanes driven by a 0.75kW servo motor. The maximum blockage amounts to 95%. A detailed description and reference measurements are published by Greenblatt [23]. The phase lag of the pressure wave which travels upstream as a result of a change in the louver position was determined to be below 1deg for all free stream velocities considered at 1Hz. Thus, all conceivable phase lags along the chord are negligible.

Figure 2 shows a schematic of the experimental setup. The two-dimensional NACA 0018 airfoil profile is placed at the vertical centre of the test section. The leading edge is positioned 0.91m downstream of the nozzle. Three-dimensional effects such as wing tip vortices are avoided by the stiff mounting of the NACA 0018 directly on the wind tunnel walls. The side walls are made of two rotatable Plexiglas windows with a diameter of 0.93m. Both windows are synchronously driven by a 1.5kW servo motor placed above the test section. This permits any arbitrary pitching motion including complete 360° loops. In all configurations, the pitching axis is located at the quarter-chord point. The unsteady free stream velocity in the test section is measured by two hotwires. The data acquisition of the surface pressures and the wind tunnel speed were synchronised, both were recorded at a frequency of 497Hz. Thus, for each unsteady pressure measurement the associated free stream velocity is recorded. The data are recorded via an anemometry system (company: *A.A. Lab Systems*, type: *AN-1003 Test Module*). The hotwires are calibrated every day before the measurements start by means of a Pitot tube above the wing. The Pitot tube measures the steady free stream velocity, which is recorded by a Dwyer Manganese pressure transducer. The hotwire probes are used to measure the unsteady oscillating free stream velocity

The wing profile centre line is equipped with 40 pressure taps with a diameter of 0.8mm to measure the static pressure at the wing surface. The pressure taps of the pressure and suction side are symmetrically distributed. This is required to determine the unsteady vorticity sheet strength which is proportional to the pressure difference at a certain chordwise position. The static pressure distribution is recorded synchronised by means of two piezoresistive pressure scanners (company: *Chell Instruments*, type: *ESP-32HD*). These two pressure scanners are placed inside the wing and each pressure port is connected to the pressure tap by a 44cm long tube. The uniform tube length may provoke a constant phase lag of the dynamic pressure measurements for all taps [26]. However, the lag of the pressure measurements was found to be negligible for the maximum oscillation frequencies of 1.2Hz considered here.

The airfoil chord is $c = 0.348$m and the span is $s = 0.61$m, resulting in an aspect ratio of 1.75. Despite this moderate aspect ratio, CFD simulation via URANS show that three-dimensional flow structures due to side wall effects are negligible at mid span [27]. At zero angle of attack, the airfoil already covers approximately 6% of the wind tunnel cross-sectional area. Nevertheless, blockage corrections during pitch motion are not calculated because the maximum angle of attack amounts to $\alpha_{max} = 4°$. Furthermore, the lift coefficient ratio is considered in the following (compare to equation 1), which eliminates the influence of a thinkable bias.

All presented quantities are normalised by means of the dynamic pressure of the free stream. Two hotwires are used to record the instantaneous free stream velocity in the test section, the instantaneous value of $u(\phi)$ is taken as the mean value of the flow speed recorded with the two probes. Any phase lags between the leading edge and the trailing edge are neg-

ligible [23]. The lift is calculated by means of the 40 pressure taps. The measured static pressure, which acts normal to the surface, is weighted by the half distance to the neighbouring pressure taps and transformed in the coordinate system of the wing chord. The summation yields the lift and the pressure drag. The cross product of the static pressure at each pressure tap and the distance to the quarter chord gives the pitch moment.

The phase reconstruction is based on the averaged free stream velocity of the two hotwires. Taking into account that the amplitude of the free stream oscillation varies slightly, each single period was fitted by an ideal sine to avoid any unphysical scatter in the data. Each measurement consists of at least 150 periods of the unsteady free stream. The data are averaged at each angle of attack $\alpha_{step} = 0.5°$ with a window size of $\pm 0.3°$ and at each phase angle $\phi_{step} = 2°$ with a window size of $\pm 1°$.

For a validation of van der Wall's theory, an accurate and reliable generation of the two sources of unsteadiness is essential. Figure 3 shows the recorded unsteady free stream velocity and the corresponding angle of attack profile which is in phase in the presented case. Additionally, an ideal sinusoidal signal is added to the measurements with the desired amplitude and frequency. This enables a direct comparison and yields the quality of adjustment. In the presented case, the theoretical unsteady free stream is $u(\phi) = (1 + 0.5\sin(\phi))13.32$m/s. The blue circles illustrate the phase averaged values. The measured mean velocity is $u_s = 13.16$m/s and the measured velocity ratio is $\sigma = 0.5098$. Only around $\phi = 60°$ and $\phi = 180°$, slightly differences from an ideal sine are detectable. The maximum relative error between the measured free stream and the ideal velocity profile is 2.5% [11]. The maximum and the minimum possess a small phase lag of approximately 4° while the crossing of the steady free stream velocity shows a phase lead of approximately -4°. The theoretical angle of attack profile is $\alpha(\phi) = 2° + 2°\sin(\phi)$. The dark green dots in figure 3 depicts the measured angle of attack (ordinate on the right hand side). The measured mean angle of attack is $\alpha_s = 2.0026°$ and the amplitude is $\alpha_{amp} = 2.009°$. As shown, the theoretical and measured angle of attack profile are almost identical and no significant differences are detectable. Furthermore, a computed cross-correlation between the measured angle of attack and the measured velocity profile exhibit a phase lag of 0°. Hence, the both functions are considered to be perfectly in phase. The high agreement of the two measured signals to an ideal sine, the reliable generation, and the good control of the phase shift show that this unsteady wind tunnel is suited for validating unsteady lift theories.

4 RESULTS: EXPERIMENTAL VALIDATION OF UNSTEADY LIFT THEORY

First of all, the in phase setup is considered according to figure 3. The free stream oscillation and the pitch motion possess the same reduced frequency k and no phase shift $\tau = 0$. Only in this case, a superposition of the two sources of unsteadiness is possible to extract the nonlinear behaviour of this oscillating system. In the following, Reynolds number effects in the experimental data are negligible as shown by Strangfeld [28].

Figure 4 shows the unsteady lift ratio at an averaged Reynolds number of $\overline{Re} = 300000$. The unsteady free stream follows the function $u(\phi) = u_s(1 + 0.5\sin(\phi))$ and the angle of attack profile is $\alpha(\phi) = 2° + 2°\sin(\phi)$. Both motions are in phase and synchronised at a frequency of $f = 1.18$Hz, which leads to a reduced frequency of $k = 0.097$. Thus, the maximum angle of attack and the maximum free stream velocity are reached at $\phi = 90°$ and their minima at $\phi = 270°$. All lift coefficients are normalised by the quasi steady lift coefficient at the mean Reynolds number and the mean angle of attack $C_l(\alpha = 2°, Re = 300000)$. The solid grey line shows the theoretical quasi steady lift coefficient. At a phase angle of $\phi = 90°$, the angle of attack is increased from $\alpha(\phi = 0°) = 2°$ to $\alpha(\phi = 90°) = 4°$, hence the normalised lift coefficient doubled up to 2. At $\phi = 270°$, the current angle of attack is zero and the resulting quasi steady lift becomes zero as well.

The black solid line in figure 4 represents the theoretical predictions of Isaacs' generalised theory as developed by van der Wall. On the one hand, van der Wall's theory predicts a lift deficit during the pitch up motion at an increasing free stream velocity compared to the quasi steady case. The maximum based on theory is $C_l(\phi = 98°)/C_{l,qs}(\alpha = 2°) = 1.87$. On the other hand, a significant lift overshoot is predicted in the range of the minimum angle of attack and free stream velocity. The minimum lift ratio based on theory is $C_l(\phi = 282°)/C_{l,qs}(\alpha = 2°) = 0.536$, although the quasi steady lift is close to zero. Considering the predicted maximum and minimum, a phase lag of around 15° to the quasi steady lift is observable. Furthermore, the experimental data are included in this plot as black dots. These phase averaged values are smoothed by means of a Fourier-series incorporating only the first two harmonics. However, the amplitude and the phase agree well with van der Wall's theory. The maximum measured lift ratio is $C_l(\phi = 98°)/C_{l,qs}(\alpha = 2°) = 1.85$ and the minimum is $C_l(\phi = 284°)/C_{l,qs}(\alpha = 2°) = 0.492$. The phase between theory and experiments is reproduced with a maximum deviation of no more than $\Delta\phi = 4°$. The close agreement between the theoretical predictions and the exerimental data suggests that Van der Wall's theory provides a very good description of the unsteady effects that produced the deviations from quasi-steady loads observed in the present experiments.

The corresponding baseline measurements allow a separated evaluation of the two unsteady effects. The blue line shows the lift coefficient ratio for an unsteady free stream at a constant angle of attack of $\alpha = 2°$. Although the wing is kept at a constant angle of attack, the unsteady inflow generates dynamic effects which affect the pressure distribution and loads as predicted by Isaacs [7]. For $0° < \phi < 180°$, the current free

stream velocity $u(\phi)$ is larger than u_s. In this range, the dynamic effects reduce the predicted lift coefficient ratio to a minimum of $C_l(\phi = 30°)/C_{l,qs} = 0.935$. At $\phi > 180°$, $u(\phi)$ is below u_s. Nevertheless, the lift ratio slope increases until a maximum lift overshoot of around 27% is reached at $\phi = 264°$. The blue dots depict the experimental data at an oscillating free stream and a constant angle of attack. The time varying lift coefficient $C_l(\phi)$ is normalised with the measured, quasi steady lift coefficient $C_{l,qs}$ of the corresponding Reynolds number (linear interpolation of 11 baseline measurements). For a better comparison of the measured dynamic effects with the theory and also for data smoothing, the measured coefficients are fitted by means of the Fourier series including only the first two harmonics [11]. In the experiments, the minimum lift is at $C_l(\phi = 50°)/C_{l,qs} = 0.926$ and the maximum lift overshoot of around 27% is reached at $\phi = 280°$. The global trend and the amplitude between Isaacs's unsteady lift theory and the experiments agree very well. Only a slightly phase shift between these two lines of approximately 18° exists.

The green line shows the unsteady lift predicted by Theodorsen [6]. The airfoil performs a sinusoidal pitch motion at a constant free stream. At a phase angle of $\phi = 0°$, the current angle of attack corresponds to the mean angle of $\alpha = 2°$ (same at $\phi = 180°$). The unsteady lift is normalised with the quasi steady lift at the mean angle of $C_{l,qs}(\alpha = 2°) = 0.219$. The maximum based on theory is reached close to the maximum angle of attack at $C_l(\phi = 92°)/C_{l,qs} = 1.85$ although the amplitude is significantly smaller compared with the quasi steady lift. The minimum lies at $C_l(\phi = 272°)/C_{l,qs} = 0.149$ and is quite far away from becoming zero. The phase averaged results are depicted as green dots. The measured unsteady lift is normalised with the measured quasi steady lift of $C_{l,qs}(\alpha = 2°) = 0.22$ The comparison of experiment and Theodorsen's theory achieves a good agreement. The small deviations of the two curves are in the range of the measurement accuracy. Hence, this experimental setup is able to reproduce the predicted lift response due to a pitch motion in a very reliable and accurate way.

However, the differential equations from van der Wall yield a nonlinear behaviour of the unsteady free stream and the pitching motion. A superposition of the pure free stream oscillation and the pure pitching motion quantifies the nonlinearity for this certain case. The solid red line illustrates the theoretical superposition. In the first half, no large differences emerge because the pure pitching motion is close to the combined case and the pure free stream oscillation does not contribute strong unsteady effects. During the second half of this oscillation $\phi > 180°$, the superposition (red) clearly deviates from the combined case (black). As expected, the nonlinear system reveals another amplitude as the superposition of the single effects. This comes from the emitted wake vorticity. The induced normal velocities on the airfoil chord possess different strengths and phase lags and nonlinearities arise. The red markers reveal the superposition of

the measured and phase averaged effects. It agrees well with the predicted values in phase and amplitude. The superposition yields almost the same effects and the same differences compared to the combined case. Thus, the nonlinear system response is reproduced well by the experiments and the observed deviations are comfortably in the range of the measurement accuracy. Thus, based on this validation, van der Wall's theory is experimentally confirmed to be able to recapture the unsteady behaviour due to pitching and high velocity ratios.

Figure 5 shows the unsteady lift response at a mean Reynolds number of $\bar{Re} = 300000$. Two cases are considered, the in phase case $\tau = 0°$ and the paraphase case $\tau = 180°$. Furthermore, two free stream velocity amplitudes of $\sigma \approx 0.33$ and $\sigma \approx 0.5$ are investigated. The measured, phase averaged time profiles of the inflow conditions are shown in the two subplots 5 (a) and (d). The green line illustrates the measured sinusoidal velocity profile for the high free stream velocity amplitude of $\sigma = 0.5$ and the red line the medium amplitude of $\sigma = 0.33$. According to the sinusoidal inflow, the angle of attack profile is phase shifted. On the left hand side at $\tau = 0°$, the angle of attack is a pure sine as well and follows the function $\alpha(\phi) = 2° + 2°\sin(\phi)$. On the right hand side, the paraphase case with depicted with $\tau = 180°$. The minimum angle of attack coincides with the highest free stream velocity and vice versa. Figure 5 (b) illustrates the in phase medium case with $\sigma = 0.34$ at a reduced frequency of $k = 0.08$. The measurements show a good agreement to the theory of van der Wall. Figure 5 (c) shows the case which was already discussed in the figure before. A comparison of 5 (b) and 5 (c) reveals a similar behaviour in the first half of the oscillation. The differences between the unsteady lift and the quasi steady lift are similar. In the second half, the $\sigma = 0.51$ case yields a higher lift ratio compared to $\sigma = 0.34$. The experimental results shown in this figure were not smoothed and thus an additional high frequency oscillation is visible at $240° < \phi < 320°$, especially at $\sigma = 0.51$. At $\sigma = 0.34$, this high frequency oscillation exists only in fragments and is significantly reduced in its amplitude. It is believed by the authors that the occurrence of a separation bubble close to the trailing edge causes these fluctuations. Besides this high frequency lift fluctuations, the measurements and the theory agree well.

Figure 5 (e) and 5 (f) reveal the results for the paraphase case at medium and high velocity oscillation amplitudes. At $\sigma = 0.33$, the measurements and the theory of van der Wall agree well. Only in the range of $290° < \phi < 330°$, the measurements deviate from the theory. A higher lift is measured and an additional high frequency oscillation is visible in this region. Thus, the suggested separation bubble close to the trailing edge might change the Kutta condition slightly and leads to the observed deviations. The $\sigma = 0.51$ case shows the same behaviour. The agreement is good except in the range of $240° < \phi < 330°$. The amplitude of the additional fluctuation becomes stronger and reveals larger deviations from the theory. To explain this phenomenon in detail, further investigations are required.

However, a comparison of the in phase and the paraphase cases yields much stronger unsteady effects for the in phase case. At $\tau = 0°$, the maximum deviation between the unsteady and the quasi steady lift coefficient is more than 0.5 at $\phi = 270°$. At $\phi = 90°$ a deviation of around 0.2 is also visible. In contrast, the paraphase cases show significantly lower differences between the unsteady and the quasi steady lift. The maximum deviation is around 0.1 at $\phi = 270°$ and $\sigma = 0.33$. At $\sigma = 0.51$, the unsteady lift tends closer to the quasi steady case. Thus, these measurements show that the phase shift of the oscillations, angle of attack and free stream, has a strong influence on the unsteady lift response which was already predicted by the theory of van der Wall.

5 CONCLUSION

This experimental investigation illustrated a number of important aspects relating to a thick airfoil subjected to pitching and surging under pre-stall conditions. Experiments conducted at large surge amplitudes, typically encountered on rotorcraft blades, proved to be a sound basis for the validation of existing theories. The comparison was satisfactory when the pitch-angle and flow velocity were in phase. However, when they were out-of-phase, the experiments exhibited a high frequency oscillation that was traced to the formation and shedding of a recirculation bubble near the trailing edge that affected the Kutta condition. This was caused by a combination low Reynolds number effects on a relatively thick (18%) airfoil. Future experiments should employ a thinner airfoil, such as a NACA 0012.

6 Acknowledgments

References

[1] S. Wagner, R. Bareiss, and G. Guidati, *Wind turbine noise*. Springer-Verlag, Berlin, 1996.

[2] J. G. Leishman, *Principles of helicopter aerodynamics*. Cambridge University Press, 2000.

[3] J. G. Leishman and A. Bagai, "Challenges in understanding the vortex dynamics of helicopter rotor wakes," *AIAA Journal*, vol. 36, no. 7, pp. 1130–1140, 1998.

[4] G. A. M. van Kuik, D. Micallef, I. Herraez, A. H. van Zuijlen, and D. Ragni, "The role of conservative forces in rotor aerodynamics," *Journal of Fluid Mechanics*, vol. 750, pp. 284–315, 2014.

[5] T. Barlas and G. Van Kuik, "Review of state of the art in smart rotor control research for wind turbines," *Progress in Aerospace Sciences*, vol. 46, no. 1, pp. 1–27, 2010.

[6] T. Theodorsen, "General theory of aerodynamic instability and the mechanism of flutter," *NACA rep., No. 496*, pp. 413–433, 1935.

[7] R. Isaacs, "Airfoil theory for flows of variable velocity," *Journal of the Aeronautical Sciences*, vol. 12, no. 1, pp. 113–117, 1945.

[8] J. M. Greenberg, "Airfoil in sinusoidal motion in a pulsating stream," tech. rep., NACA TN1326, 1947.

[9] B. G. van der Wall, "The influence of variable flow velocity on unsteady airfoil behavior," tech. rep., DLR-FB 92-22, Braunschweig, Germany, 1992.

[10] B. G. van der Wall and J. G. Leishman, "On the influence of time-varying flow velocity on unsteady aerodynamics," *Journal of the American Helicopter Society*, vol. 39, no. 4, pp. 25–36, 1994.

[11] C. Strangfeld, H. Müller-Vahl, C. N. Nayeri, C. O. Paschereit, and D. Greenblatt, "Unsteady aerodynamics of an airfoil in an oscillating free stream," in *7th AIAA Theoretical Fluid Mechanics Conference, AIAA Aviation, Atlanta, Georgia*, 2014.

[12] J. G. Leishman, "Challenges in modelling the unsteady aerodynamics of wind turbines," in *21st ASME Wind Energy Symposium and the 40th AIAA Aerospace Sciences Meeting, Reno, Nevada*, 2002.

[13] D. Favier, A. Agnes, C. Barbi, and C. Maresca, "Combined translation/pitch motion-a new airfoil dynamic stall simulation," *Journal of Aircraft*, vol. 25, no. 9, pp. 805–814, 1988.

[14] K. Granlund, B. Monnier, M. Ol, and D. Williams, "Airfoil longitudinal gust response in separated vs. attached flows," *Physics of Fluids*, vol. 26, no. 2, pp. 1–14, 2014.

[15] N. Ham, P. Bauer, and T. Lawrence, "Wind tunnel generation of sinusoidal lateral and longitudinal gusts by circulation of twin parallel airfoils," *NASA STI/Recon Technical Report N*, vol. 75, pp. 29–51, 1974.

[16] G. A. Pierce, D. L. Kunz, and J. B. Malone, "The effect of varying freestream velocity on airfoil dynamic stall characteristics," *Journal of the American Helicopter Society*, vol. 23, no. 2, pp. 27–33, 1978.

[17] J. P. Retelle, J. M. McMichael, and D. A. Kennedy, "Harmonic optimization of a periodic flow wind tunnel," *Journal of Aircraft*, vol. 18, no. 8, pp. 618–623, 1981.

[18] A. Szumowski and G. Meier, "Forced oscillations of airfoil flows," *Experiments in Fluids*, vol. 21, no. 6, pp. 457–464, 1996.

[19] S. Harding, G. Payne, and I. Bryden, "Generating controllable velocity fluctuations using twin oscillating hydrofoils: experimental validation," *Journal of Fluid Mechanics*, vol. 750, pp. 113–123, 2014.

[20] D. Favier, J. Rebont, and C. Maresca, "Large-amplitude fluctuations of velocity and incidence of an oscillating airfoil," *AIAA Journal*, vol. 17, no. 11, pp. 1265–1267, 1979.

[21] M. Goodrich and J. Gorham, "Wind tunnels of the western hemisphere," in *Federal Research Division Library of Congress, Washington, DC*, pp. 81–82, 2008.

[22] K. Gompertz, C. Jensen, P. Kumar, D. Peng, J. W. Gregory, and J. P. Bons, "Modification of transonic blowdown wind tunnel to produce oscillating freestream mach number," *AIAA Journal*, vol. 49, no. 11, pp. 2555–2563, 2011.

[23] D. Greenblatt, "Unsteady low-speed wind tunnel design," in *31st AIAA Aerodynamic Measurement Technonoly & Ground Testing Conference, Dalls, Texas*, 2015.

[24] R. Isaacs, "Airfoil theory for rotary wing aircraft," *Journal of the Aeronautical Sciences*, vol. 13, no. 4, pp. 218–220, 1946.

[25] J. D. Anderson, *Fundamentals of Aerodynamics*. McGraw-Hill Education, Singapore, 2011.

[26] D. Greenblatt, J. Kiedaisch, and H. Nagib, "Unsteady-pressure corrections in highly attenuated measurements at moderate mach numbers," in *31st AIAA Fluid Dynamics Conference & Exhibit, Anaheim, California*, 2001.

[27] C. Strangfeld, C. L. Rumsey, H. Müller-Vahl, D. Greenblatt, C. N. Nayeri, and C. O. Paschereit, "Unsteady thick airfoil aerodynamics: experiments, computation, and theory," in *45th AIAA Fluid Dynamics Conference, Dallas, Texas*, 2015.

[28] C. Strangfeld, *Active control of trailing vortices by means of long- and short-wavelength actuation*. PhD thesis, Technische Universität Berlin, 2015.

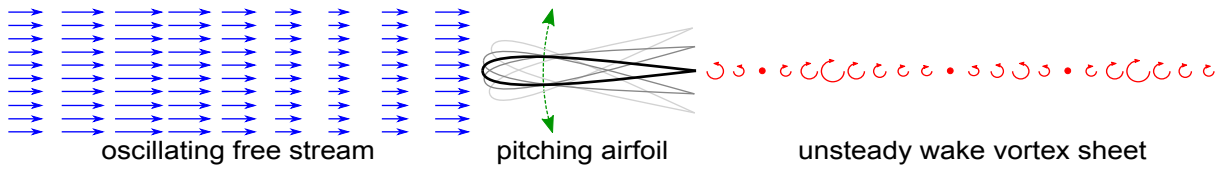oscillating free stream   pitching airfoil   unsteady wake vortex sheet

Figure 1: Sketch of a pitching airfoil in an oscillating free stream which generates an unsteady wake vortex sheet
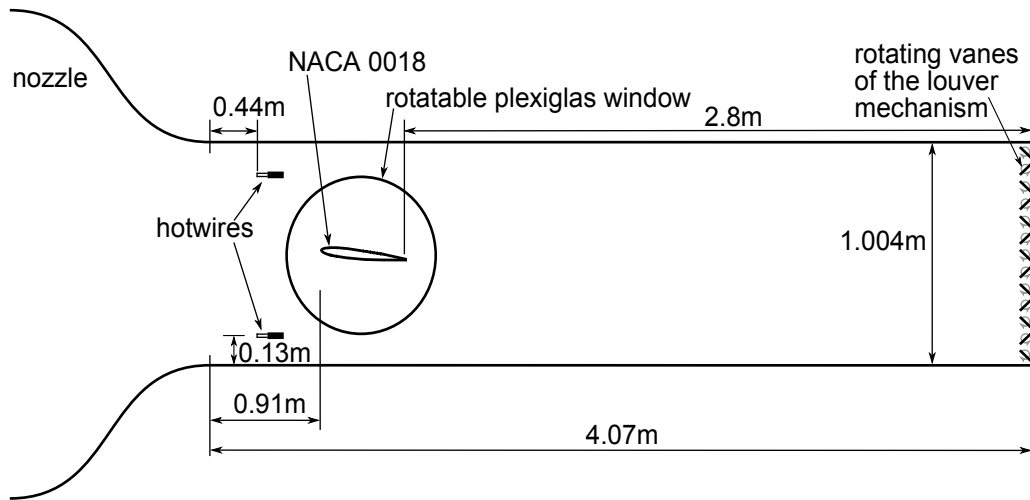

Figure 2: Sketch of the wind tunnel setup: The louver mechanism is placed at the end of the wind tunnel. The wing is rotatable and the unsteady free stream velocity is recorded upstream of the wing via two hotwires.
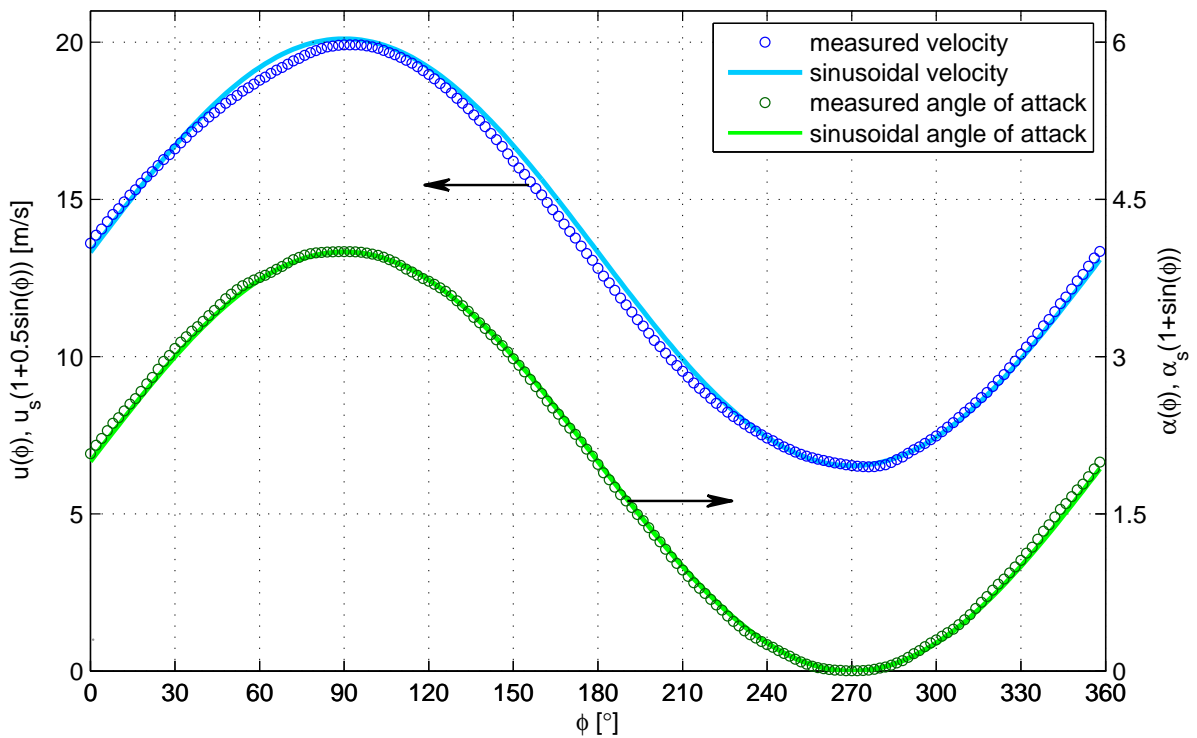

Figure 3: Comparison of the measured free stream velocity (dark blue circles) and the measured angle of attack (dark green circles); the ideal sinusoidal functions $u(\phi) = (1 + 0.5\sin(\phi))13.32$m/s and $\alpha(\phi) = 2° + 2°\sin(\phi)$ are depicted as solid lines
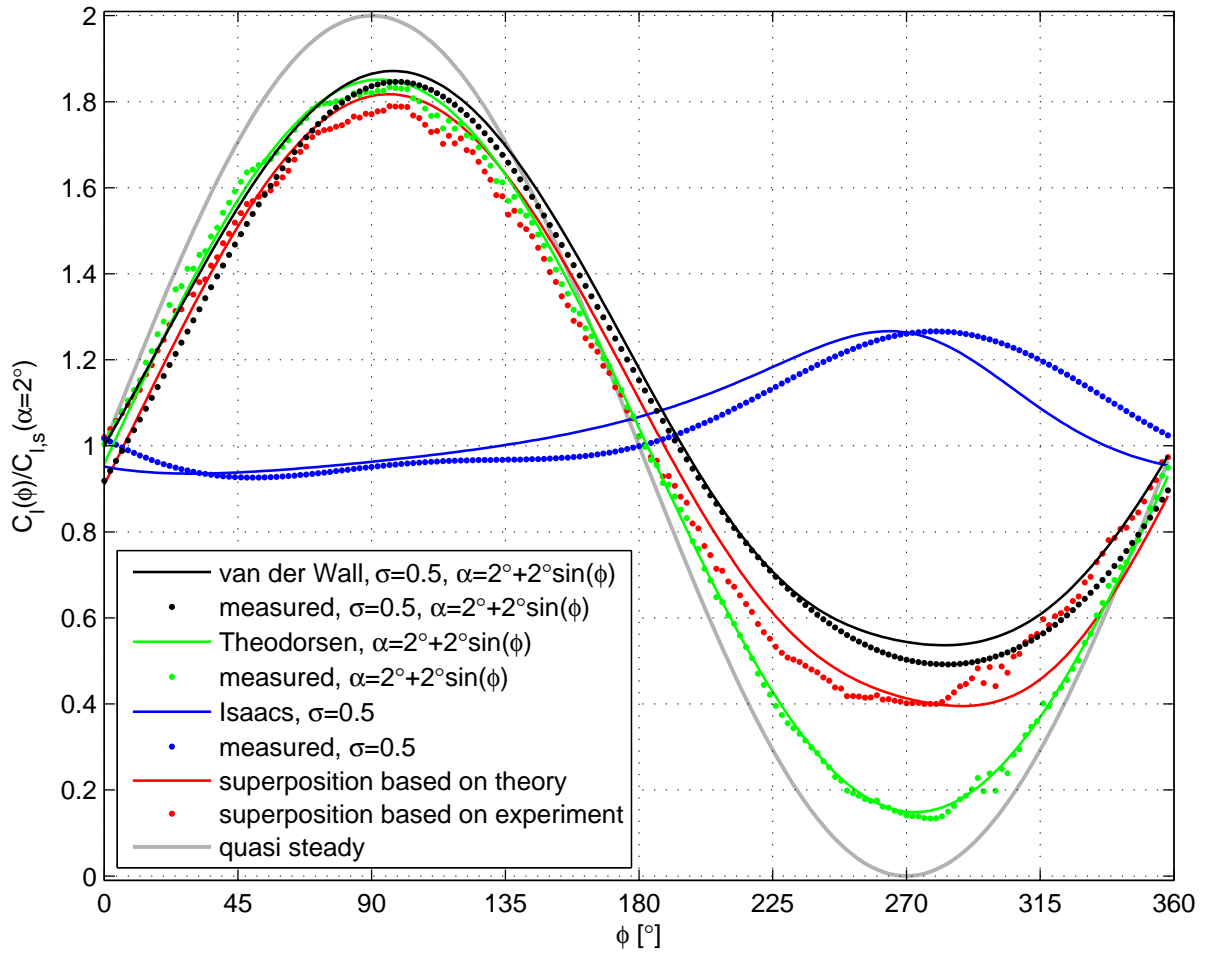
Figure 4: Comparison of theoretical predictions (solid lines) and experimental results (dots) at synchronized, simultaneous pitch motion $\alpha(\phi) = 2° + 2° \sin(\phi)$ and free stream oscillations $u(t) = u_s(1 + 0.5 \sin(\phi))$, $\overline{Re} = 300000$, $k = 0.097$
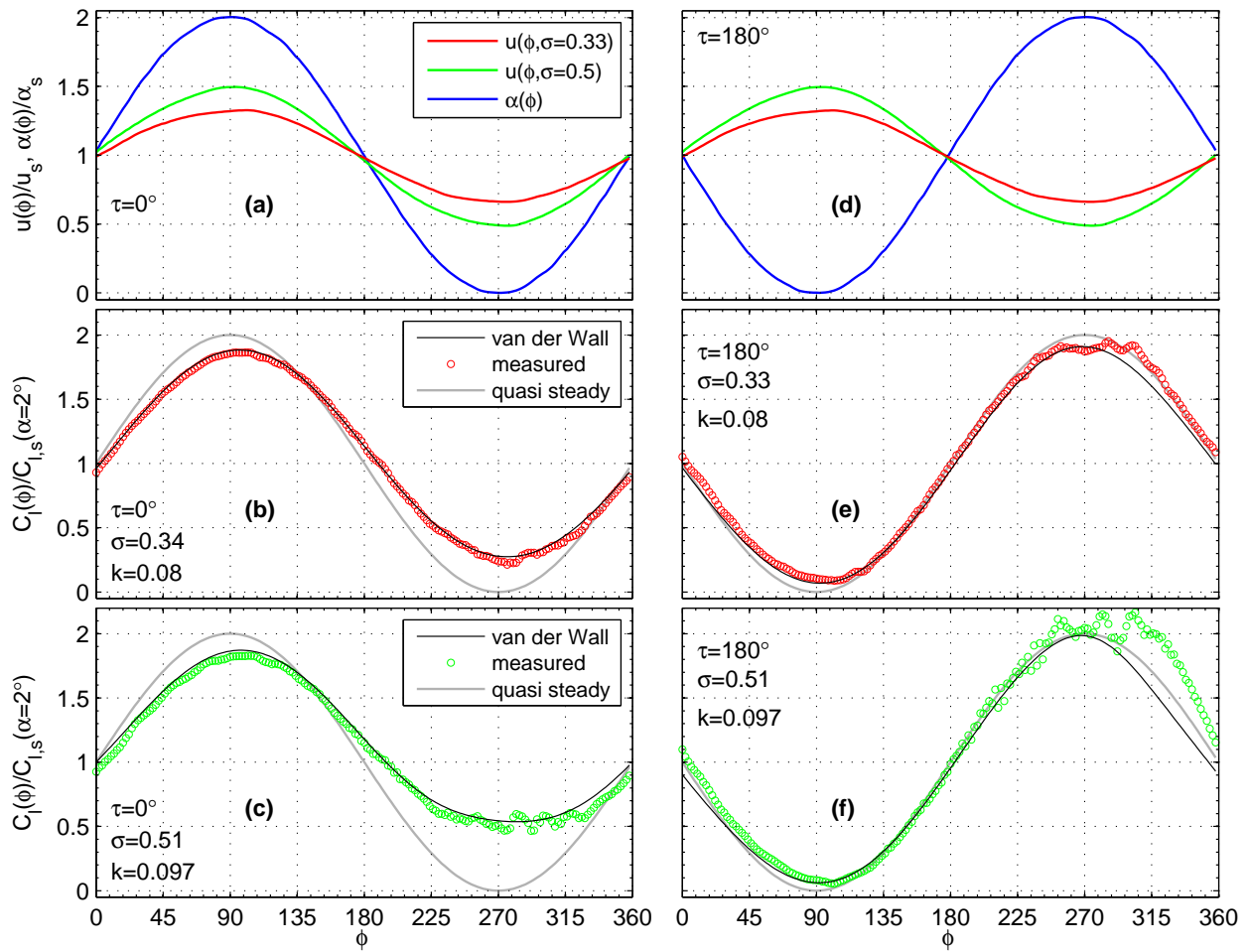
Figure 5: Unsteady lift ratio during synchronized, simultaneous pitching $\alpha(\phi) = 2° + 2° \sin(\phi)$ and oscillating free stream $u(t) = u_s(1 + \sigma \sin(\phi))$ for two phase shifts of $\tau = 0°$ and $\tau = 180°$ and variable free stream velocity amplitudes of $\sigma \approx 0.33$ and $\sigma \approx 0.5$, $k = 0.08$ or $k = 0.097$, $\overline{Re} = 300000$